IEEE Access
Multidisciplinary | Rapid Review | Open Access Journal

Received July 10, 2020, accepted July 27, 2020, date of publication July 30, 2020, date of current version August 18, 2020.

Digital Object Identifier 10.1109/ACCESS.2020.3013011

Modified-Segmented Split-Ring Based Polarization and Angle-Insensitive Multi-Band Metamaterial Absorber for X, Ku and K Band Applications

SAIF HANNAN[1], MOHAMMAD TARIQUL ISLAM[1], (Senior Member, IEEE), NORSUZLIN MOHD SAHAR[2], KAMARULZAMAN MAT[1], MUHAMMAD E. H. CHOWDHURY[3], (Member, IEEE), AND HATEM RMILI[4], (Senior Member, IEEE)

[1]Department of Electrical, Electronic and Systems Engineering, Faculty of Engineering and Built Environment, Universiti Kebangsaan Malaysia, Bangi 43600, Malaysia
[2]Space Science Center (ANGKASA), Universiti Kebangsaan Malaysia, Bangi 43600, Malaysia
[3]Department of Electrical Engineering, Qatar University, Doha 2713, Qatar
[4]Department of Electrical and Computer Engineering, Faculty of Engineering, King Abdulaziz University, Jeddah 21589, Saudi Arabia

Corresponding authors: Saif Hannan (p98220@siswa.ukm.edu.my), Mohammad Tariqul Islam (tariqul@ukm.edu.my), and Hatem Rmili (hatem.rmili@yahoo.fr)

This work was supported by the Science and Technology Unit, King Abdulaziz University, Saudi Arabia, under award number (١٠٣-٤١-ع-و).

ABSTRACT A novel modified-segmented split-ring based symmetric metamaterial absorber is introduced in this paper for X, Ku, and K band applications. The perfect absorption was achieved with a total of 1.91 GHz absorption bandwidth using the conventional FR4 substrate without resistive lumped elements. EM waves were applied in TEM mode at both normal and oblique incidence up to 90° and the same absorptance was found at 11.23 GHz, 14.18 GHz, 17.37 GHz, and 19.18 GHz with the maximum of 85.51%, 99.13%, 98.19%, and 90.8% absorptance respectively. This absorption performance was proved for both co- and cross-polarization analysis. Double negative values of permittivity and permeability up to 17.37 GHz and single negative values of either permittivity or permeability at 19.18 GHz were achieved. An equivalent circuit analysis also proved its performance capability, which makes it a perfect metamaterial absorber. Finally, the comparison of the design with recently published works in terms of unit cell size, absorption band, maximum polarization angles, and cross-polarized absorptivity proved it as a better candidate for the potential use as a perfect absorber.

INDEX TERMS Wideband, metamaterial absorber, modified segmented split-ring, X Ku and K band, triple band.

I. INTRODUCTION

Metamaterials have recently received significant attention from communities of science and engineering due to many applications. The metamaterials play a vital role, especially when used as absorbers in the case of electromagnetic (EM) waves. Metamaterial (MM) absorbers are those engineered devices, which may exhibit a negative value of either permittivity or permeability or both are negative [1]. As a consequence, the incident EM wave through the absorber will suffer from the negative value of the refractive index [2]; which traps the incident EM wave inside the absorber. A lot of work is underway to develop perfect MM absorbers to perform for different applications like absorber integrated with antennae for noise reduction [3], remote sensing applications [4], microwave imaging [5], stealth technologies especially for military vehicles [6], reducing radar cross-sections [7], [8], invisibility cloaking [9] and SAR reduction [10], [11]. Generally, a specially designed precise patch or an array of patches on one side of a dielectric substrate

The associate editor coordinating the review of this manuscript and approving it for publication was Wanchen Yang.

and a ground of the same material of the patch set at the other side of the substrate is used for MM absorber design [12]. Usually, annealed copper is used for patch and ground for most of the absorbers but the substrate material is the major concern of designing a perfect MM absorber. Research is underway to develop various substrate materials to fabricate perfect MM absorbers. Though the developed substrates are unique, they are hard to fabricate commercially and handy for installing in EM wave appliances. Hence commercially available substrates (like FR4, Rogers RT, or RO) are being used in recent times for their universal applicability and availability [13]–[15].

Sharp peaks in absorptance with a very narrow bandwidth of EM waves are common for mostly designed MM absorber with FR4 substrates to date. It is a challenge to achieve a wide bandwidth of absorption frequency using FR4 substrates [16], [17]. As FR4 is the most popular substrate for MM absorber design, many designs are published although a few of them have shown perfect absorption analysis by both co-polar and cross-polarized EM waves. Moreover, equivalent circuit analysis is rarely found in these papers. Although FR4 is a lossy material (dielectric constant = 4.3), it can be used for higher frequencies due to its interesting behavior at higher frequencies [18]–[20]. In this paper, we propose a wide-angle polarization-insensitive perfect MM absorber using the traditional FR4 substrate. Both co-polar (normal and oblique incidence) and cross-polar analysis were done along with equivalent circuit analysis. A total of 1.91 GHz absorption was achieved with more than 70% absorption margin considering −10dB value of S parameters. Moreover, absorption peaks were found in X, Ku, and K frequency bands with 0.2 GHz, 0.93 GHz, and 0.78 GHz frequency bandwidths respectively; with double negative (DNG) values in peaks at X and Ku bands and single negative (SNG) value at K band.

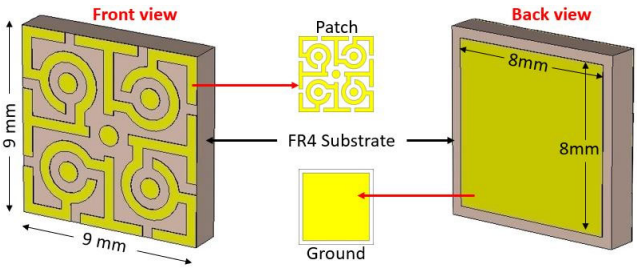

FIGURE 1. The designed unit cell.

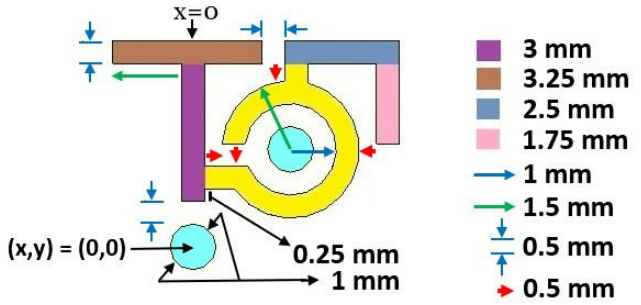

FIGURE 2. The detailed dimension of a segment resonator.

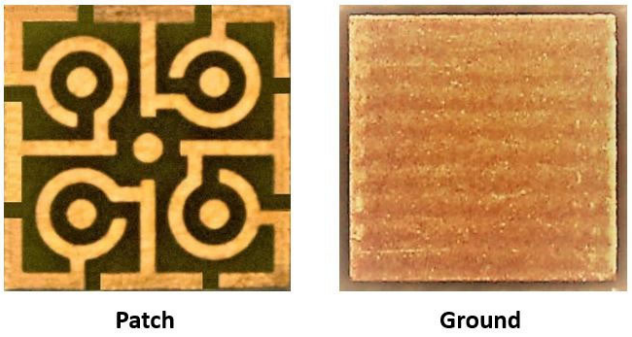

FIGURE 3. The fabricated unit cell.

II. UNIT CELL DESIGN AND FABRICATION

The unit cell was designed on an FR4 substrate of a thickness of 1.6 mm and area $9mm \times 9mm$. The patch and the ground are on the two opposite surfaces of the substrate. The patch and the ground are of annealed copper (lossy) of thickness 0.035 mm as shown in figure 1. The patch consists of four quadrants of similar shapes. Each quadrant has a circular split ring with a circular dot at the center (shown in figure 2). A similar circular dot is at the center of the unit cell surrounded by the quadrants. The entire patch is four-fold symmetric with two splits on each borderline. The width of the slits and the copper strips are 0.5mm. Also, the diameter of all the circular dots is 1 mm. The ground has an area of $8mm \times 8mm$. Figure 1 depicts the structure of the unit cell in detail.

The split rings with unique shaped strips act as independent resonators (shown in figure 2). All four resonators simultaneously act at different resonance frequencies. The periodicity of the unit cell was achieved by considering the theory of Wood's anomaly for EM wave absorptions by plane surfaces [21] and the size of the unit cell was determined. The transmission lines of all inductive copper strips work for surface current passage whereas the gaps act as capacitive loads to maintain electric dipoles to be immersed and distributed in between the copper strips in the dielectric substrate material. As the purpose of the unit cell is to absorb almost the entire incident EM wave at different frequencies, no reflection and transmission of EM wave through the cell is expected. The designed patch expectedly may not reflect the incident EM wave because of its design is not entirely a solid metal (copper) surface. On the other hand, it should not allow transmission of the incident EM waves through it. Hence, a solid copper surface at the opposite side of the patch was chosen, as the metal surface acts as a reflector to EM waves. The ground area was varied and set to the value and the position as shown in figure 1, for the best absorption performance. The unit cell was fabricated as shown in figure 3.

The unit cell was designed on CST 2017 software installed in a computer with Intel® Core i5-8250 CPU with 3.4 GHz clock speed and 8 GB RAM. The average time for simulations for normal and oblique incidences took around 12-13 minutes

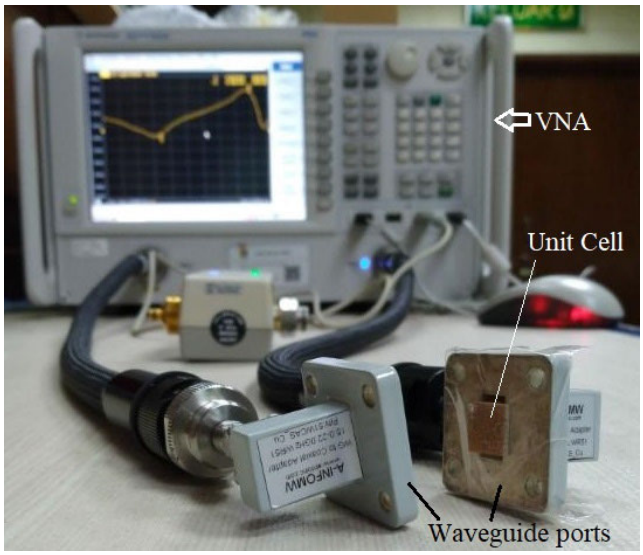

FIGURE 4. Experimental setup for unit cell measurement.

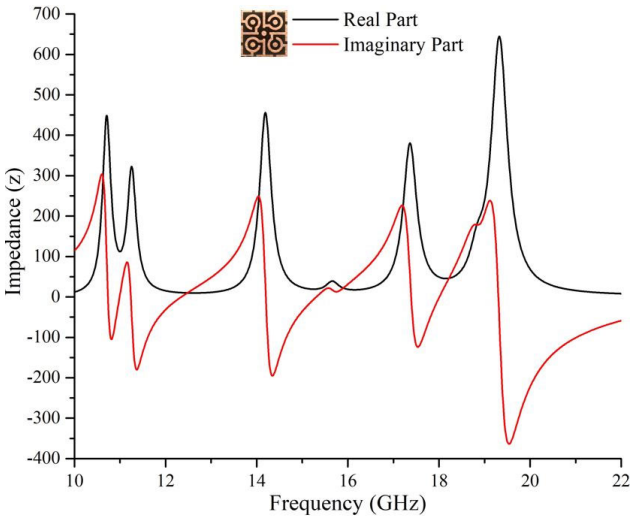

FIGURE 5. The impedance of the unit cell at different applied frequencies (from simulation).

to extract S_{11} and S_{21} parameters. The S parameters were saved in Microsoft Excel files and were used in Matlab 2018a by appropriate codes to find the results. Two waveguide ports were set up at the front and backside of the unit cell at 0°, 45°, and 90° angles. During the simulation, perfect electric field and perfect magnetic fields were set along x- and y-directions and EM waves were applied along the z-direction. Transverse electric and magnetic (TEM) mode of operation was used.

After getting satisfying results in the simulation, the unit cell was fabricated as shown in figure 3. Its performances were tested by PNA network analyzer N5227A as shown in figure 4. Two different waveguide ports were used in the measurement process (one for 10-15 GHz and other for 15-22 GHz). The data found from these ports were combined to get final data (total number of points are the same with simulation) and were compared with simulated data.

III. FUNDAMENTALS OF THE ABSORBER AND METHODOLOGY

An absorber will absorb EM waves perfectly if there is no reflection and transmission through the absorber. The perfect absorption can be understood by the following equation 1.

$$\mathrm{A}(\omega) = 1 - \Gamma(\omega) - \mathrm{T}(\omega) \tag{1}$$

where, $\Gamma(\omega) = |S_{11}(\omega)|^2$ is the reflection coefficient and $\mathrm{T}(\omega) = |S_{21}(\omega)|^2$ is the transmission coefficient. As the proposed design has a copper ground (which is a pure conductor), there will be a very negligible amount of transmission through the absorber. Also, the reflection of the incident EM wave from the absorber is negligible because of the following equation 2.

$$\Gamma(\omega) = \frac{Z_{MM}(\omega) - Z_0}{Z_{MM}(\omega) + Z_0} \tag{2}$$

where, Z_{MM} is the impedance of the MM absorber and Z_0 is the free space impedance. The input impedance Z_{MM} of the MM absorber can be expressed as

$$Z_{MM} = \sqrt{\frac{\mu_0 \mu_r(\omega)}{\epsilon_0 \epsilon_r(\omega)}} \tag{3}$$

Here, μ_0 and ϵ_0 are the permeability and permittivity constant of free space and $\mu_r(\omega)$ and $\epsilon_r(\omega)$ are the frequency-dependent relative permeability and relative permittivity, respectively. Hence free space impedance,

$$Z_0 = \sqrt{\frac{\mu_0}{\epsilon_0}} \approx 377\Omega \tag{4}$$

If $Z_{MM} = Z_0$, there will be no reflection of the incident EM wave from the absorber as per equation 2. Hence absorption will be maximum. The scenario can be imagined in figure 5.

The absorptance, S_{11} and S_{21} parameters (simulated) of the proposed absorber are plotted in figure 6.

It can be understood from these figures that at the resonance frequencies (11.23 GHz, 14.18 GHz, 17.37 GHz, and 19.18 GHz), the reflection and transmission coefficients are near to zero. Hence highest absorptance (simulated) was found at these frequencies as per equation 1.

IV. RESULTS AND ANALYSIS

The optimum performance of the proposed absorber unit cell was ensured by the evolution in the patch design as shown in figure 7. To get the maximum number of resonance peaks, more SRRs were incorporated into the same unit cell size that obeyed Wood's anomaly rule for plane FSS [22].

The patch was first designed by an SRR (split-ring resonator) with a circular dot at the center. As absorption by this design was not satisfactory, the patch was further improvised with multiple SRRs (2^{nd} design) and the absorption performance was increased but not to the expected level. Then a square boundary ring with four arms aimed at the center of the unit cell was introduced (3^{rd} design), but both high

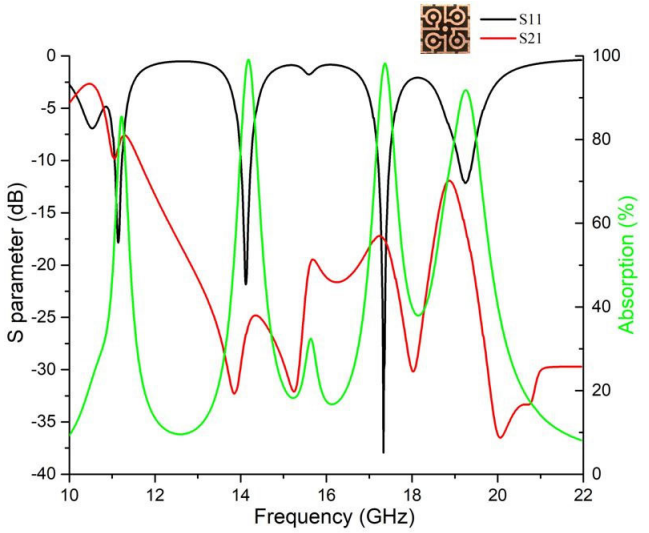

FIGURE 6. Absorptance, S_{11} and S_{21} parameters of the proposed absorber (from simulation).

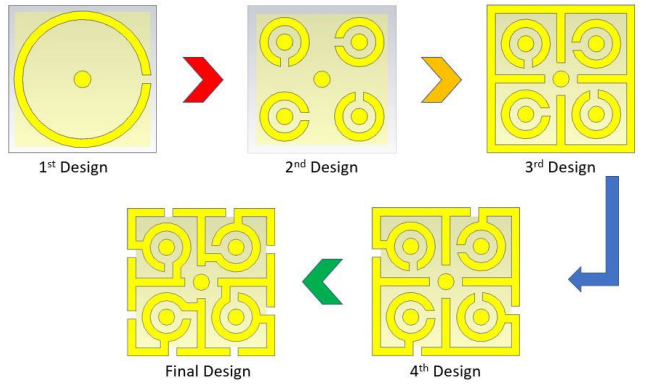

FIGURE 7. Evolution of the unit cell for optimum performance.

absorption and negative value of permittivity/permeability were not achieved. To increase absorption and maintain negativity, some splits were introduced in the square ring (4th design). In this case, double negative values were achieved but absorptivity decreased. Finally, the patch was improvised with more capacitive and inductive elements ending up with the final patch design, which performed maximum absorption with DNG properties as shown in figures 8(a), 8(b), 8(c) & 9, by green curves. The size of the final design was proven fit by the Bragg's law of EM wave diffraction rule followed by unit cell size within $\lambda/4$.

The step by step improvement in the performance of the unit cell is explained by figures 8(a), 8(b), 8(c) & 9, as per figure 7. It can be seen from figure 8 that, at resonance frequencies (11.23 GHz, 14.18 GHz, 17.37 GHz, and 19.18 GHz), the values of permittivity, permeability and refractive index are negative for design 5. Also, at these resonance frequencies, absorptance is found maximum for design 5.

All the values considered for figure 8 (for only the real parts) and figure 9 are taken from the simulation.

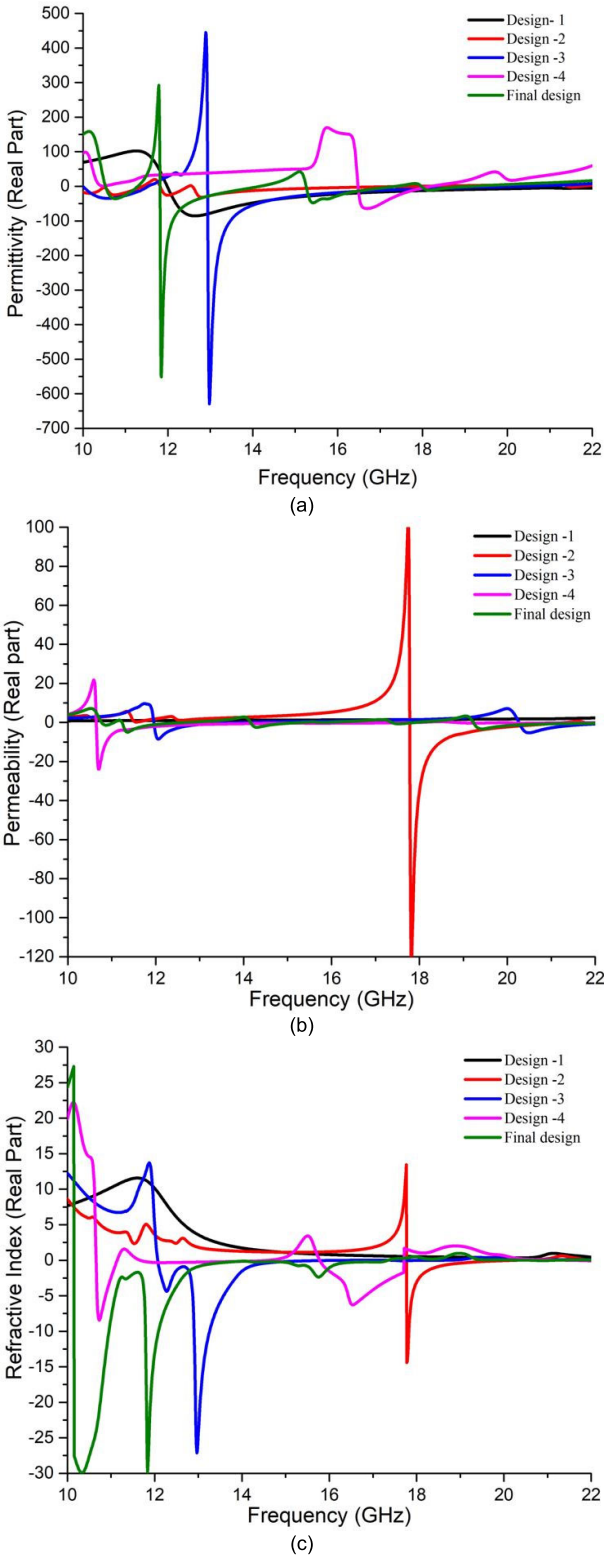

FIGURE 8. Performance evolution of the patch as per figure 7 for (a) relative permittivity, (b) relative permeability and (c) refractive index (real parts) with respect to frequency.

The proposed MM absorber unit cell was simulated under the normal incidence of the EM waves at 0°, 45°, and 90° from both the waveguide ports. The values of relative

TABLE 1. Performance indicators of the proposed absorber at different polarizing angles in tem mode.

Frequency Bands	Polarizing angle	Resonance Frequencies GHz	Bandwidth GHz	Relative Permittivity	Relative Permeability	Refractive Index (NRW)	Refractive Index (DRI)	Absorption %
X	0°	11.23	**0.2**	-4.379	-1.09	-2.369	-2.369	**85.51**
Ku		14.18	**0.44**	-0.1342	-0.2407	-0.1812	-0.1812	**99.1**
		17.37	**0.49**	-0.0037	-0.0047	-0.0043	-0.0043	**98.19**
K		19.18	**0.78**	-0.1345	3.112	-1.073	1.073	**90.56**
X	45°	11.23	**0.2**	-3.81	-1.677	-2.391	-2.391	**85.38**
Ku		14.18	**0.45**	0.0149	-0.4627	-0.1908	-0.1894	**99.13**
		17.37	**0.49**	0.1482	-0.1203	-0.0152	0.0134	**98.14**
K		19.18	**0.77**	-0.0774	3.087	-1.075	1.075	**90.8**
X	90°	11.23	**0.2**	-3.395	-1.432	-2.383	-2.391	**85.38**
Ku		14.18	**0.45**	0.0489	-0.4627	-0.1908	-0.1894	**99.13**
		17.37	**0.49**	0.1482	-0.1104	-0.0135	0.0135	**98.14**
K		19.18	**0.77**	-0.0774	3.096	-1.075	1.075	**90.8**

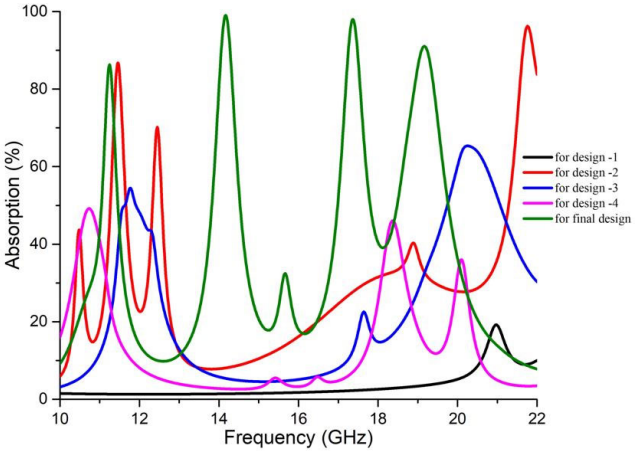

FIGURE 9. Absorption performance as per figure 7.

permittivity, relative permeability; refractive indices by both the Nicolson-Ross-Weir (NRW) and the Direct Refractive Index (DRI) method were calculated along with absorptivity. Absorption bandwidth was achieved considering -10dB values of both reflection and transmission coefficients, which was observed with more than 70% absorptance.

All these values were calculated from S_{11} and S_{21} parameters, as listed in table 1. From table 1, it is evident that the simulated results show double negative (DNG) characteristics of both permittivity and permeability at 11.23 GHz, 14.18 GHz, and 17.37 GHz at normal incidence and 11.23 GHz for 45° and 90° polarized EM wave. Moreover, single negative (SNG) properties of either permittivity or permeability were achieved for 19.18 GHz at all polarizing angles and 14.18 GHz and 17.37 GHz for both 45° and 90° incident waves. As a result, the refractive index was found negative (either by NRW or DRI method or both) at all the resonance frequencies for each polarization angles, as followed by equations (5) & (6).

$$= -real\left[\sqrt{\epsilon_r\ \mu_r}\right] \quad \text{(by NRW method)} \tag{5}$$

$$\text{and } = \text{real}\left[\frac{c}{i\pi f t}\sqrt{\frac{(S_{21}-1)^2-(S_{11})^2}{(S_{21}-1)^2+(S_{11})^2}}\right] \text{ (By DRI method)} \tag{6}$$

In equation (6), c is the speed of light, f is the frequency of applied EM wave and t is the thickness of the substrate. Equations [1 to 6] are standard equations derived from [23].

The results are depicted in figures 10 & 11.

To extract effective permittivity and permeability in the TEM mode of simulation, both real and imaginary values of these parameters were considered since the unit cell has SRRs [24]. As negative values of imaginary parts of the permittivity and permeability calculated from S parameters can be due to numerical errors in simulation [25], thus imaginary parts were not considered for these figures.

It can be observed from these two figures that, the values of permittivity, permeability, and refractive index found from the simulation are not matched with measured values, especially at lower frequencies. This was because of the fact that measurement setup with the waveguide port for lower frequency range had probable mechanical or electrical sensitivity errors during measurement which was unavoidable. At higher frequencies, the simulated and measured values are almost similar. It is essential to mention that, the values are almost the same at all the resonance frequencies as can be seen from figures 10 & 11.

Hence the proposed absorber was claimed a strong candidate for MM absorber with a maximum of 85.85%, 99.13 %, 98.19%, and 90.8% absorptance at 11.23 GHz, 14.18 GHz, 17.37 GHz, and 19.18 GHz resonance frequencies respectively. The absorption found from the simulation at all polarized incident waves for normal and oblique incidences in TEM mode are compared in figures 12 (a) & 12 (b).

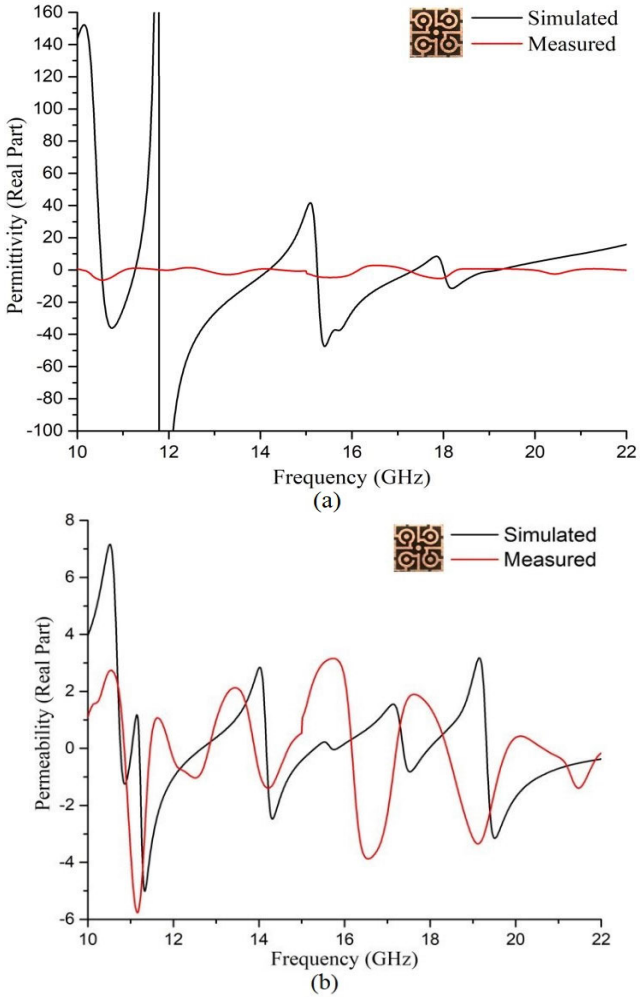

FIGURE 10. Variation in simulation and measurement for (a) permittivity and (b) permeability.

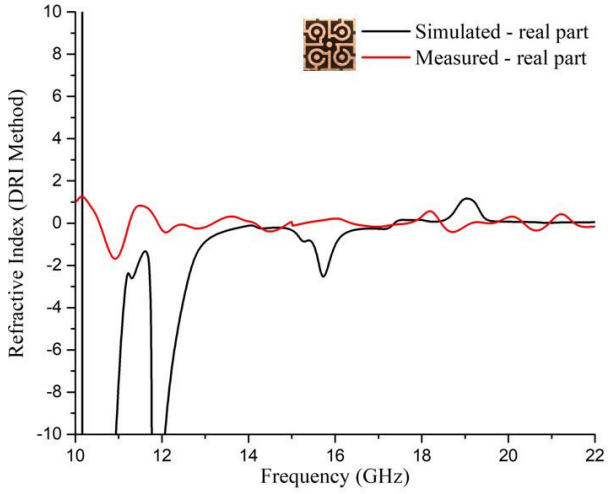

FIGURE 11. Simulated and measured refractive index.

The bandwidth of absorption was considered from the lowest and the highest value of frequencies with more than 70% absorptivity (corresponding to −10dB value of S parameters),

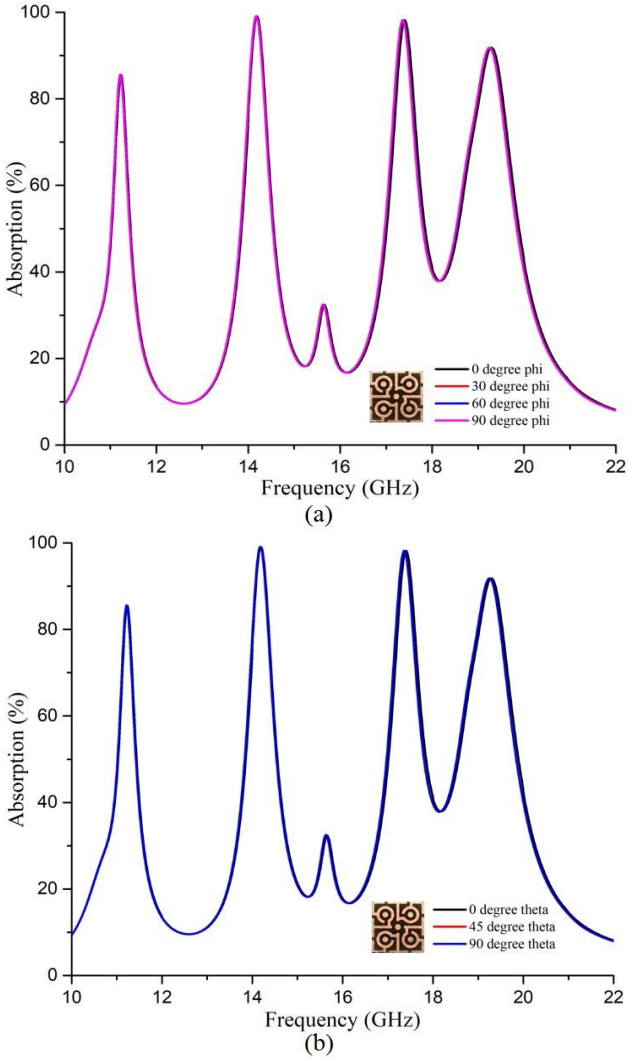

FIGURE 12. Absorptance (simulated) at different polarized EM waves in TEM mode for (a) normal incidence (b) oblique incidence.

before and after each maximum absorption peak respectively. On average, a total of 1.91 GHz of incident EM wave was absorbed effectively out of 12 GHz total incident EM wave on the proposed absorber unit cell at all polarizing angles. Moreover, the frequency range covers X, Ku, and K bands, as depicted in table 1.

A very slight deviation in resonance frequency is observed for the higher band, but the overall absorption performance remains the same for all polarizing angles. The absorption bandwidth of the proposed MM unit cell was achieved by taking the summation of the frequency spans about each resonance peak with a maximum of -10dB value of the corresponding reflection and transmission coefficients.

As absorption depends not only on co-polarized EM waves but also on cross-polarization elements of EM waves and hence, equation 1 should be modified. Since the proposed unit cell has a solid copper ground, the transmission coefficient can be neglected. Moreover, the reflection coefficient due to co-polarized and cross-polarized EM waves are important.

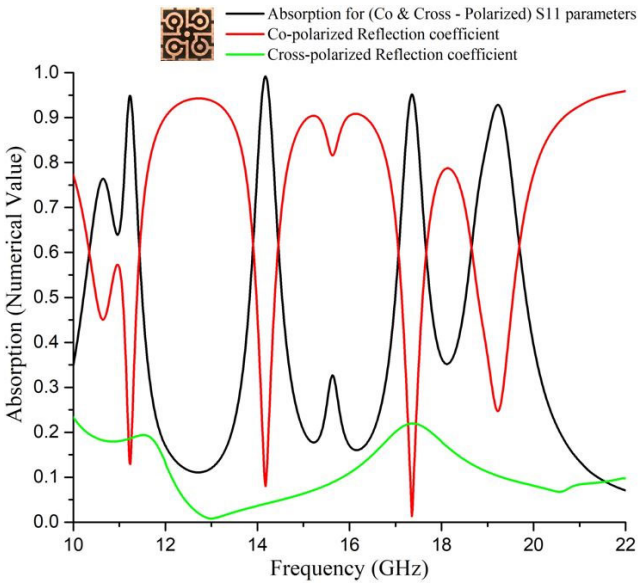

FIGURE 13. Absorptance considering both co & cross-polarized reflection coefficients in normal incidence (simulated).

Thus, equation 1 becomes

$$A = 1 - \left[\left| S_{11}^{Co}(\omega) \right|^2 - \left| S_{11}^{Cross}(\omega) \right|^2 \right] \tag{7}$$

where, $\left|S_{11}^{Co}(\omega)\right|^2$ is the reflection coefficient due to the co-polarized wave and $\left|S_{11}^{Cross}(\omega)\right|^2$ is the reflection coefficient due to the cross-polarized wave [26].

In figure 13, the absorption capability of the proposed unit cell considering equation 7 is shown. Floquet ports with TE (transverse electric) and TM (transverse magnetic) mode was used for the simulation in this case. The cross-polarized reflection coefficient has an insignificant influence on absorptivity as per figure 13 and hence proves the unit cell as polarization insensitive.

The reasons behind the maximum absorptance found at 11.23 GHz, 14.18 GHz, 17.37 GHz, and 19.18 GHz can be explained in figure 14 below. The surface current distribution, the electric and the magnetic fields at these resonance frequencies are found distinctive in this figure.

For better understanding, surface current distributions are shown for both the patch and the ground by red arrows. At the resonance frequencies, the intensity of the fields varied over different segment resonators of the unit cell. The reference scales were found from simulation for normal incidence. As declared earlier, perfect electric and perfect magnetic fields were set along the x-axis and y-axis respectively. Along the z-axis, the EM waves were applied from both the +z axis and -z-axis. Hence, the current distribution, the electric, and the magnetic fields shown in figure 14 at perspective views are the z-components of respective fields due to applied waves.

Out of the four resonance frequencies, maximum absorption (99.13 %) was found at 14.18 GHz and minimum absorption (85.38%) was found at 11.23 GHz. At these two resonance frequencies and 17.37 GHz, DNG values of both permittivity and permeability were achieved, which can be understood by the surface current distribution of the patch and the ground. The direction of current distributions of the ground is found parallel with the inductive copper strips on the patch at these frequencies. The SRRs have created a circular path of current flow which led to a magnetic response, which can be seen from corresponding 14 (d) figures. The corresponding electric field distributions in figure 14 (c) show that the excited positive charges (red regions) are circulating negative charges (blue regions), which act as an electric dipole. The opposite circulating direction of the diagonal SRRs on the patch led to electric coupling that tends to electric dipole moment, as a result, magnetic resonance is found. Hence EM absorptance at these frequencies can be imagined due to electric and magnetic responses. The DNG values can be found from S_{11} parameters at these frequencies considering equations 8 and 9, below.

$$\epsilon_{eff} = 1 + \frac{2j}{k_o d}\left(\frac{1 - S_{11}}{1 + S_{11}}\right) \tag{8}$$

$$\mu_{eff} = 1 + \frac{2j}{k_o d}\left(\frac{1 + S_{11}}{1 - S_{11}}\right) \tag{9}$$

where, ϵ_{eff} is effective permittivity and μ_{eff} is the effective permeability of the proposed absorber. k_o is the wavenumber of air medium and d is the thickness of the substrate [27]. The value of S_{11} in these equations are taken for normal incidence. As transmission coefficient has very small values at the resonance frequencies, so S_{21} parameters are ignored.

At 19.18 GHz, it can be seen from figure 14 that, the direction of surface current on the patch and the ground are anti-parallel by half of the path at each SRR but parallel at the linear square-shaped strip at the center of the patch area. This led to the electric current coupling at each SRR except the center square strips. Hence absorption is found but magnetic dipoles are not formed perfectly. Hence effective permeability was found positive and effective permittivity was found negative due to electric dipoles. So, SNG properties are found at this frequency. The field distributions in figure 14 for all the resonance frequencies can be correlated with the above explanations.

Figure 14 (a) shows that the central circular copper dot has less influence on the surface current density at all resonance frequencies. The absorptance of the absorber unit cell will, therefore, be the same without this dot, but from figure14(c) the central circular dot shows the direction of the non-resonant electrical field which is ultimately the direction of the magnetic dipoles as can be correlated with figure14(d). This is why the central dot was kept in the design.

The change of the magnetic field is perpendicular to the electric field. Hence it is lagging behind the electric field. So, the places (in the unit cell) with high electric fields instantaneously shows less magnetic fields and vice-versa. That means the magnetic fields are polarized. This is because of the magnetic dipoles that are aligned along with magnetic fields.

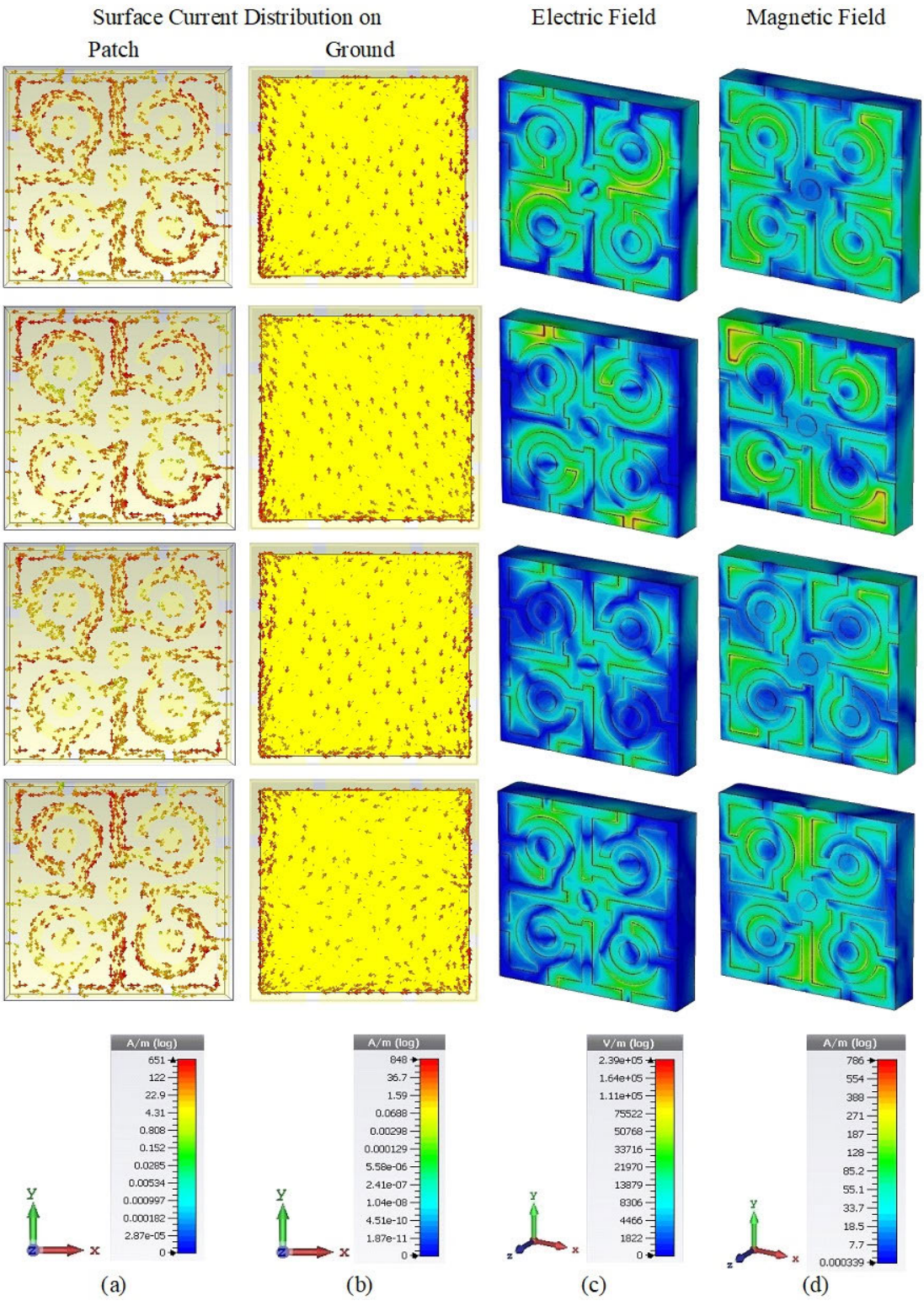

FIGURE 14. Snapshots of distributions of (a & b) surface current, (c) electric field and (d) magnetic field at 11.23 GHz, 14.18 GHz, 17.37 GHz, and 19.18 GHz respectively.

So, the energy of the waves due to incident magnetic fields are trapped and thus will be less reflection of incident EM waves and maximum absorption inside the lossy dielectric material.

The equivalent circuit of the unit cell is shown in figure 15 below, as the equivalent circuit approach [27]–[31] is essential for proving the absorber as perfect MM absorber.

TABLE 2. Comparison of the proposed absorber with recently published works.

Design	Absorptance in Frequency Bands	Patch type	Maximum absorption (%)	Thickness of unit cell (mm)	Unit cell size (mm)	Max polarizing angle insensitivity (for both normal and oblique incidence)	Both co- and cross-polarization insensitivity	Efficient microwave energy harvesting and other applications
				λ_o is the wavelength of the lowest frequency for the highest absorption				
Ref [33]	X	Square SRR	99.92 %	3.2 mm (0.065 λ_o)	9 mm (0.26 λ_o)	Up to 45°	No	Not possible
Ref [27]	Ku	Square SRR	99.8 %	1.6 mm (0.064 λ_o)	3.65 mm (0.36 λ_o)	Up to 60°	No	Not possible
Ref [34]	K	Square SRR	99.98 %	0.635 mm (0.041 λ_o)	6 mm (0.39 λ_o)	Up to 85°	No	Not possible
Ref [35]	X and Ku	Circular SRR	99.66 %	2 mm (0.061 λ_o)	7.1 mm (0.22 λ_o)	Up to 15°	No	Not possible
Ref [36]	X and Ku	Circular SRR	96.7%	1.6 mm (0.054 λ_o)	12 mm (0.41 λ_o)	Up to 45°	No	Not possible
Ref [37]	X and Ku	Split Jerusalem cross	99.9 %	0.8 mm (0.027 λ_o)	12 mm (0.41 λ_o)	Up to 60°	No	Not possible
Ref [38]	C, X, and Ku	Modified square SRR	97.15 %	1 mm (0.055 λ_o)	8 mm (0.19 λ_o)	Up to 60°	No	Not possible
Ref [39]	X, Ku, and K	Circular SRR	99 %	1.6 mm (0.087 λ_o)	6.6 mm (0.36 λ_o)	Up to 45°	No	Not possible
This Work	X, Ku, and K	Modified circular SRR	99.13 %	1.58 mm (0.059 λ_o)	9 mm (0.34 λ_o)	Up to 90°	Yes	Possible

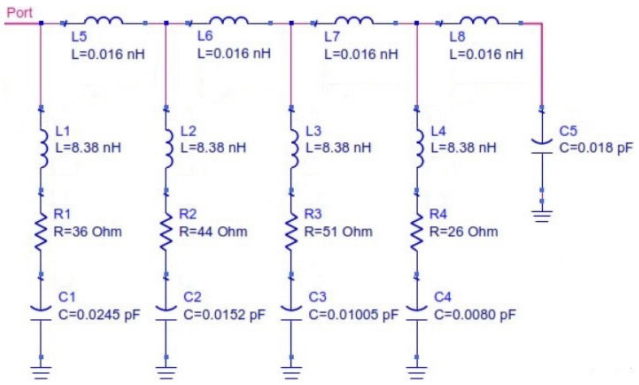

FIGURE 15. Equivalent circuit of the unit cell.

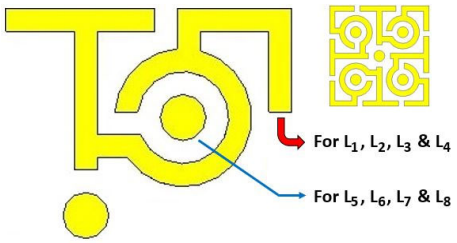

FIGURE 16. Independent inductors of the patch.

For each resonance frequency, an LRC circuit connected with the port, and the ground was designed. As the unit cell has a solid copper ground, the transmission coefficient is negligible (as can be understood from figure 18 (b)) and thus only one port was chosen for the circuit input. Each segment (as shown in figures 2 and 16) acts as an independent partial resonator with the remaining 3 segments. Each segment resonator has some resistance and capacitance. The values of all components are shown in figure 15. L5, L6, L7, and L8 act as parallel inductors due to circular copper dots on the patch except for the center dot, as shown in figure 16. The center copper dot of the unit cell has less influence on surface current distributions as can be seen from figure 14. The ground has a capacitance (C5 in figure 15) due to its circumferential etching (as shown in figures 1 and 3) and the gap due to the substrate thickness. This etching was required to get resonance peaks with maximum absorption rate. The surface currents on the ground (for this etching) diverged to the active segment resonator arms through the conductive gap due to the substrate, as the substrate acted as potential well for the surface current elements.

The inductance and capacitance of the circuit were determined following the microstrip LC circuit and LRC circuit theory [32] as shown in equations 10 & 11.

$$L_{SR} = 0.00508L\left[\ln\left(\frac{2L}{W+D}\right)+0.5+0.2235\frac{(W+D)}{L}\right] \quad (10)$$

where, $\mathbf{L_{SR}}$ is the inductance (in $\boldsymbol{\mu H}$) of the polygonal split-ring microstrip as shown in figure 17, W is the width (in inch) of the strip, L is the length (in inch) of the copper strip and D is the distance between the patch and the ground.

$$C = \frac{1}{4\pi^2 f^2 L_{SR}} \quad (11)$$

where, C is the gross capacitance (in pF) for resonance frequency f (in GHz) and associated inductance $\mathbf{L_{SR}}$. Hence for four resonance frequencies, C has four values as per equation 11, as shown in figure 15.

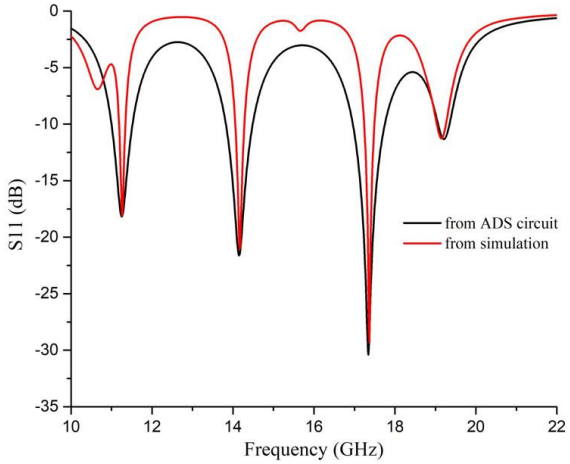

FIGURE 17. The reflection coefficient of the unit cell from the equivalent circuit and simulation.

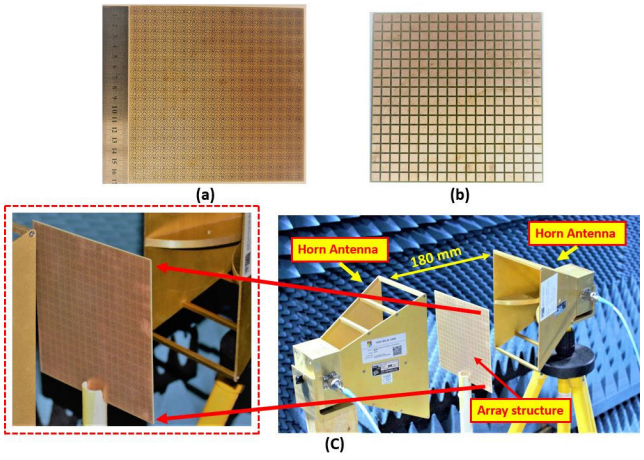

FIGURE 18. Fabricated structure of the 18 × 18 array (a) patch and (b) ground; (c) measurement setup of the array structure with horn antenna.

The equivalent circuit was designed on ADS software. The resistance (R_1, R_2, R_3, R_4, etc.) for each resonance frequency was achieved by varying the values to match the simulated S_{11} parameter value (in dB) for corresponding resonance frequency.

Finally, the reflection coefficient (S_{11}) was extracted from the ADS circuit and plotted in figure 17 along with simulated S_{11} and was found identical at the resonance frequencies.

V. ARRAY PERFORMANCE ANALYSIS

The design was fabricated as an 18 × 18 array structure as shown in figure 18 (a). The patch was backed up by a ground with conductive circumference for each unit cell as can be seen from figure 18 (b). Before measurement, a raw copper plate was placed in between the horn antennas to assume the standard reflection for incident EM waves. The array structure was placed in between two horn antennas set apart by 180 mm in an anechoic chamber as depicted in figure 18 (c). The same VNA was used to measure the reflection and transmission coefficients of the fabricated array. The EM waves were set to propagate along z-direction considering the 0- phi polarizing angle to ensure normal incidence.

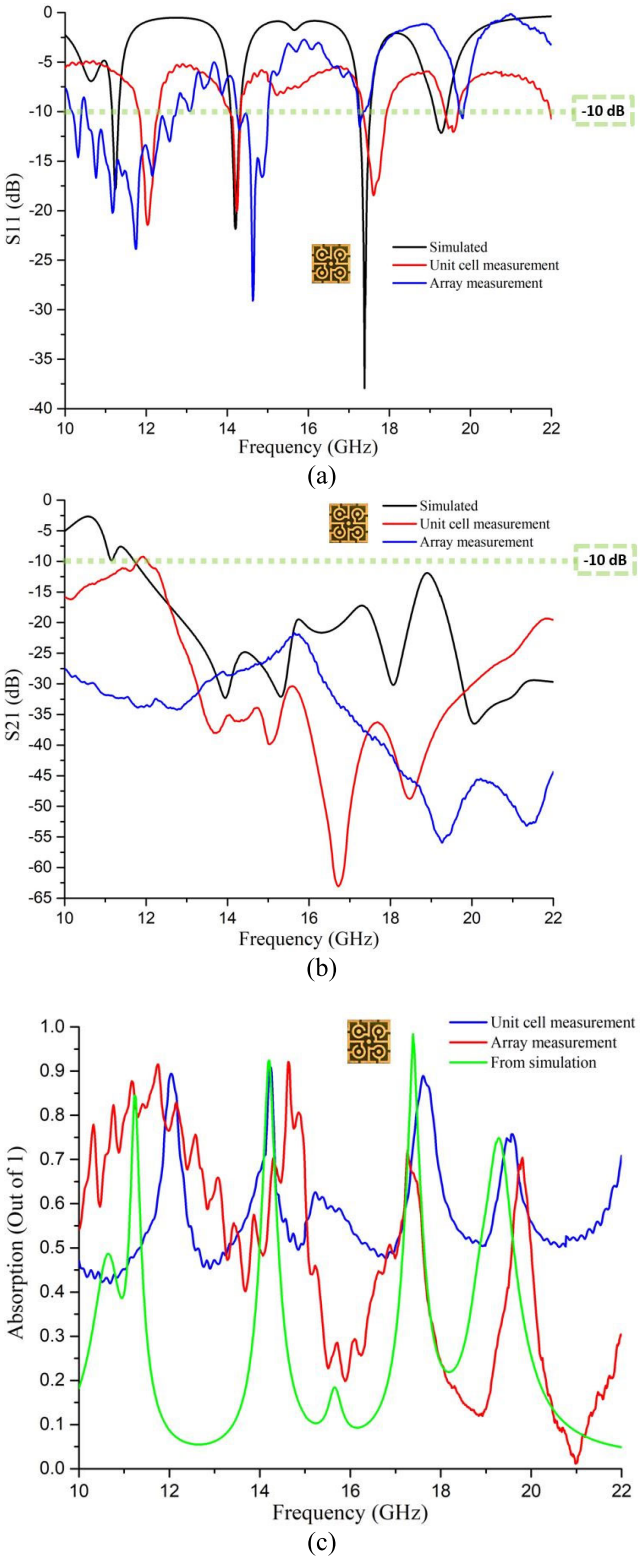

FIGURE 19. Comparison of the measured (a) S_{11} parameter, (b) S_{21} parameter and (c) absorption of the unit cell and array with simulation.

The measured S11, S21, and absorption of the array are shown in figure 19.

For convenience, the corresponding measured values for the unit cell are also included in the figure. It can be observed from figure 19 that for the array structure of the proposed absorber, absorption bandwidth is greater than that of the unit cell and the simulation at lower frequency (X band). For the Ku band, absorption was found with quite large bandwidth than unit cell and simulation, whereas for higher frequency (K band), the array showed less absorptance than unit cell and simulation. Hence the proposed design shows a good absorptance with DNG values at lower frequencies and SNG values at higher frequencies. The deviation from the simulated resonance points might be due to mutual coupling among the unit cells of the fabricated array, less perfect connecting cables from VNA to horn antennas or due to fabrication error in the array prototype, but both the array and the unit cell achieved perfect absorptance at X, Ku and K bands.

From above all discussions, the performance of the proposed MM absorber can be understood. Moreover, a quantitative comparison is required in terms of the performance indicators, with recently published works. Hence table 2 is introduced with all relevant comparison parameters and relevant works done with FR4 substrate with no lumped resistor in the patch. It is now clear from table 2 that, our design is best in terms of a unique shaped patch, highest absorption with less unit cell area, maximum polarization angle insensitivity for both normal and oblique incidence, and above all, insensitive to both co-polar and cross-polar incident EM waves. It is essential to inform that, all the references in table-2 have absorptance at higher frequencies (X, Ku Bands) but the proposed absorber has shown perfect absorptance at X, Ku, and K bands with FR4 substrate.

VI. CONCLUSION

A novel MM absorber with FR4 substrate was introduced in this paper, which has shown very good absorptance with double negative (DNG) properties in X and Ku bands and single negative (SNG) properties in the K band. In addition, it has polarization insensitivity up to 90°, and due to structural symmetry of the patch and the ground, it is angle-insensitive for both normal and oblique incidence. Four distinct resonances were found at 11.23 GHz, 14.18 GHz, 17.37 GHz, and 19.18 GHz by both simulation and practical measurements. Above all, the design has shown a perfect absorption with a total bandwidth of 1.91 GHz within −10dB limits, which is verified by both co- and cross-polarization analysis. An equivalent circuit was also designed to get the idea of the microstrip line transmission genre of the unit cell. The measured values for unit cell and array have coincided with the simulation results in most cases. This significant performance of the design can make it a proper candidate for future employment in many microwave applications at X, Ku, and K band. The absorber can be embedded into electronic devices used in space crafts or satellites where EM energy can be converted into electrical energy from unnecessary EM signals received from different orbiting satellites. This energy from the absorber can be used for charging batteries of the spacecraft or satellite. Moreover, it can be employed in numerous fields of EM wave applications like EMC (electromagnetic compatibility) & EMI (electromagnetic interference) suppression and spectrum identification, antenna noise reduction at higher frequencies, signal detection, radar imaging, satellite communications, etc.

ACKNOWLEDGMENT

This project was funded by Science and Technology Unit - King Abdulaziz University – Kingdom of Saudi Arabia – award number (١٠٣-٤١-ع و).

REFERENCES

[1] N. I. Landy, S. Sajuyigbe, J. J. Mock, D. R. Smith, and W. J. Padilla, "Perfect metamaterial absorber," *Phys. Rev. Lett.*, vol. 100, May 2008, Art. no. 207402.

[2] R. A. Shelby, "Experimental verification of a negative index of refraction," *Science*, vol. 292, no. 5514, pp. 77–79, Apr. 2001.

[3] P. Garg and P. Jain, "Isolation improvement of MIMO antenna using a novel flower shaped metamaterial absorber at 5.5 GHz WiMAX band," *IEEE Trans. Circuits Syst. II, Exp. Briefs*, vol. 67, no. 4, pp. 675–679, Apr. 2020.

[4] S. Jiang, Q. Zong, and X. Deng, "Application analysis of GPS positioning technology and GIS based on metamaterial in forestry engineering," in *Proc. E3S Web Conf.*, vol. 118, 2019, p. 03059.

[5] M. Islam, M. Islam, M. Samsuzzaman, M. Faruque, and N. Misran, "A negative index metamaterial-inspired UWB antenna with an integration of complementary SRR and CLS unit cells for microwave imaging sensor applications," *Sensors*, vol. 15, no. 5, pp. 11601–11627, May 2015.

[6] H. Chen, W. Ma, Z. Huang, Y. Zhang, Y. Huang, and Y. Chen, "Graphene-based materials toward microwave and terahertz absorbing stealth technologies," *Adv. Opt. Mater.*, vol. 7, no. 8, Apr. 2019, Art. no. 1801318.

[7] D. Winson, B. Choudhury, N. Selvakumar, H. Barshilia, and R. U. Nair, "Design and development of a hybrid broadband radar absorber using metamaterial and graphene," *IEEE Trans. Antennas Propag.*, vol. 67, no. 8, pp. 5446–5452, Aug. 2019.

[8] Y. Fan, J. Wang, X. Fu, Y. Li, Y. Pang, L. Zheng, M. Yan, J. Zhang, and S. Qu, "Recent developments of metamaterials/metasurfaces for RCS reduction," *EPJ Appl. Metamaterials*, vol. 6, p. 15, Jan. 2019.

[9] G. Zhao, S. Bi, M. Niu, and Y. Cui, "A zero refraction metamaterial and its application in electromagnetic stealth cloak," *Mater. Today Commun.*, vol. 21, Dec. 2019, Art. no. 100603.

[10] M. R. I. Faruque, M. T. Islam, and N. Misran, "Electromagnetic (EM) absorption reduction in a muscle cube with metamaterial attachment," *Med. Eng. Phys.*, vol. 33, no. 5, pp. 646–652, Jun. 2011.

[11] M. Hasan, M. Faruque, S. Islam, and M. Islam, "A new compact double-negative miniaturized metamaterial for wideband operation," *Materials*, vol. 9, no. 10, p. 830, Oct. 2016.

[12] J. Y. Rhee, Y. J. Kim, C. Yi, J. S. Hwang, and Y. P. Lee, "Recent progress in perfect absorbers by utilizing metamaterials," *J. Electromagn. Waves Appl.*, vol. 34, no. 10, pp. 1–34, Sep. 2019.

[13] S. Hannan, M. T. Islam, A. Hoque, M. J. Singh, and A. F. Almutairi, "Design of a novel double negative metamaterial absorber atom for Ku and K band applications," *Electronics*, vol. 8, no. 8, p. 853, Jul. 2019.

[14] N. T. Q. Hoa, T. S. Tuan, L. T. Hieu, and B. L. Giang, "Facile design of an ultra-thin broadband metamaterial absorber for C-band applications," *Sci. Rep.*, vol. 9, no. 1, p. 468, Dec. 2019.

[15] S. Hannan, M. T. Islam, A. F. Almutairi, and M. R. I. Faruque, "Wide bandwidth Angle- and polarization-insensitive symmetric metamaterial absorber for X and Ku band applications," *Sci. Rep.*, vol. 10, no. 1, pp. 1–9, Dec. 2020.

[16] P. Yu, L. V. Besteiro, Y. Huang, J. Wu, L. Fu, H. H. Tan, C. Jagadish, G. P. Wiederrecht, A. O. Govorov, and Z. Wang, "Broadband metamaterial absorbers," *Adv. Opt. Mater.*, vol. 7, no. 3, 2019, Art. no. 1800995.

[17] M. Hossain, M. Faruque, M. Islam, and K. Mat, "A new compact octagonal shape perfect metamaterial absorber for microwave applications," *Appl. Sci.*, vol. 7, no. 12, p. 1263, Dec. 2017.

[18] F. Ahmadi and N. Ida, "A broadband ultrathin metamaterial absorber using tilted parallel strips," in *Terahertz, RF, Millimeter, and Submillimeter-Wave Technology and Applications X*, vol. 10103. Bellingham, WA, USA: SPIE, 2017, Art. no. 101031V.
[19] T. Liu and S.-S. Kim, "Ultrawide bandwidth electromagnetic wave absorbers using a high-capacitive folded spiral frequency selective surface in a multilayer structure," *Sci. Rep.*, vol. 9, no. 1, pp. 1–10, Dec. 2019.
[20] N. Misran, S. H. Yusop, M. T. Islam, and M. Y. Ismail, "Analysis of parameterization substrate thickness and permittivity for concentric split ring square reflectarray element," *J. Eng.*, vol. 23, pp. 11–16, Nov. 2012.
[21] D. Maystre, "Theory of Wood's anomalies," in *Plasmonics*. Cham, Switzerland: Springer, 2012, pp. 39–83.
[22] C. Yi, Y. J. Yoo, Y. J. Kim, K. W. Kim, Y. Lee, and J. Y. Rhee, "Role of Wood's anomaly in the performance of metamaterial absorbers with periodicity comparable to wavelength," *J. Phys. D, Appl. Phys.*, vol. 49, no. 19, May 2016, Art. no. 195103.
[23] I. Brener, S. Liu, I. Staude, J. Valentine, and C. Holloway, *Dielectric Metamaterials: Fundamentals, Designs and Applications*. Cambridge, U.K.: Woodhead Publishing, 2019.
[24] D. H. Lee and W. S. Park, "Extraction of effective permittivity and permeability of periodic metamaterial cells," *Microw. Opt. Technol. Lett.*, vol. 51, no. 8, pp. 1824–1830, Aug. 2009.
[25] J. Woodley and M. Mojahedi, "On the signs of the imaginary parts of the effective permittivity and permeability in metamaterials," *JOSA B*, vol. 27, no. 5, pp. 1016–1021, 2010.
[26] L. Dong, B. Zhang, J. Duan, Y. Yang, Y. Liu, Y. Xu, H. Xu, and B. Chen, "Conformal transparent metamaterials inducing ultra-broadband absorption and polarization conversion," *J. Infr., Millim., Terahertz Waves*, vol. 40, no. 9, pp. 905–916, Sep. 2019.
[27] J. B. O. de Araujo, G. L. Siqueira, E. Kemptner, M. Weber, C. Junqueira, and M. M. Mosso, "An ultrathin and ultrawideband metamaterial absorber and an equivalent-circuit parameter retrieval method," *IEEE Trans. Antennas Propag.*, vol. 68, no. 5, pp. 3739–3746, May 2020.
[28] F. Costa, S. Genovesi, A. Monorchio, and G. Manara, "A circuit-based model for the interpretation of perfect metamaterial absorbers," *IEEE Trans. Antennas Propag.*, vol. 61, no. 3, pp. 1201–1209, Mar. 2013.
[29] S. Bhattacharyya, S. Ghosh, and K. V. Srivastava, "Equivalent circuit model of an ultra-thin polarization-independent triple band metamaterial absorber," *AIP Adv.*, vol. 4, no. 9, Sep. 2014, Art. no. 097127.
[30] C. F. Zhang, G. Q. Jing, and X. X. Xu, "Simple prediction of tunable metamaterial absorbers reflectivity characteristics using equivalent circuit model," in *Advanced Materials Research*, vol. 875. Cham, Switzerland: Trans Tech Publ, 2014, pp. 957–961.
[31] F. Bagci and F. Medina, "Design of a wide-angle, polarization-insensitive, dual-band metamaterial-inspired absorber with the aid of equivalent circuit model," *J. Comput. Electron.*, vol. 16, no. 3, pp. 913–921, Sep. 2017.
[32] O. Wing, *Classical Circuit Theory*. Cham, Switzerland: Springer, 2008.
[33] P. Ranjan, A. Choubey, S. K. Mahto, R. Sinha, and C. Barde, "A novel ultrathin wideband metamaterial absorber for X-band applications," *J. Electromagn. Waves Appl.*, vol. 33, no. 17, pp. 2341–2353, Nov. 2019.
[34] S. Ramya and I. S. Rao, "Bandwidth enhanced nearly perfect metamaterial absorber for K-band applications," in *Microelectronics, Electromagnetics and Telecommunications*. Cham, Switzerland: Springer, 2016, pp. 27–34.
[35] S. Ghosh, S. Bhattacharyya, D. Chaurasiya, and K. V. Srivastava, "An ultrawideband ultrathin metamaterial absorber based on circular split rings," *IEEE Antennas Wireless Propag. Lett.*, vol. 14, pp. 1172–1175, 2015.
[36] M. Bağmancı, O. Akgöl, M. Özaktürk, M. Karaaslan, E. Ünal, and M. Bakır, "Polarization independent broadband metamaterial absorber for microwave applications," *Int. J. RF Microw. Comput.-Aided Eng.*, vol. 29, no. 1, Jan. 2019, Art. no. e21630.
[37] P. Jain, A. K. Singh, J. K. Pandey, S. Garg, S. Bansal, M. Agarwal, S. Kumar, N. Sardana, N. Gupta, and A. K. Singh, "Ultra-thin metamaterial perfect absorbers for single-/dual-/multi-band microwave applications," *IET Microw., Antennas Propag.*, vol. 14, no. 5, pp. 390–396, Apr. 2020.
[38] D. Sood and C. C. Tripathi, "Quad band electric field-driven LC resonator-based polarisation-insensitive metamaterial absorber," *IET Microw., Antennas Propag.*, vol. 12, no. 4, pp. 588–594, Mar. 2018.
[39] S. Bhattacharyya, "An ultra-thin wide-angle cross polarization conversion metasurface with enhanced bandwidth," in *Proc. Int. Symp. Antennas Propag. (ISAP)*, Oct. 2017, pp. 1–2.

SAIF HANNAN received the B.Sc. and M.S. degrees in physics from the Shahjalal University of Science & Technology, Bangladesh, in 2007 and 2009, respectively. He is currently pursuing the Ph.D. degree with Universiti Kebangsaan Malaysia (UKM). He has been serving with the International Islamic University Chittagong (IIUC) as a Faculty Member, since 2011. His research interests include VLSI system design, natural language processing, microwave, millimeter-wave metamaterial absorber design, antenna for 5G, and so on.

MOHAMMAD TARIQUL ISLAM (Senior Member, IEEE) is currently a Professor with the Department of Electrical, Electronic and Systems Engineering, Universiti Kebangsaan Malaysia (UKM), and also a Visiting Professor with the Kyushu Institute of Technology, Japan. He is the author and coauthor of about 500 research journal articles, nearly 175 conference papers, and a few book chapters on various topics related to antennas, metamaterials, and microwave imaging with 20 inventory patents filed. Thus far, his publications have been cited 6000 times and his H-index is 38 (Source: Scopus). His Google scholar citation is 8200 and H-index is 42. He has supervised about 30 Ph.D. theses, 20 M.Sc. theses, and has mentored more than ten postdocs and Visiting scholars. He was a recipient of more than 40 research grants from the Malaysian Ministry of Science, Technology and Innovation, Ministry of Education, UKM research grant, and international research grants from Japan and Saudi Arabia. His research interests include communication antenna design, satellite antennas, and microwave imaging. He has also been serving as an Executive Committee member for the IEEE AP/MTT/EMC Malaysia Chapter, since 2018, a Chartered Professional Engineer (CEng), a member of IET, U.K., and a Senior Member of IEICE, Japan. He received several International Gold Medal awards, a Best Invention in Telecommunication Award for his research and innovation, and best researcher awards, in 2010 and 2011, at UKM. He was a recipient of the 2018 and 2019 IEEE AP/MTT/EMC Malaysia Chapter, Excellent Award. He also won the Best Innovation Award in 2011 and the Best Research Group in ICT niche in 2014 by UKM. He was a recipient of Publication Award from Malaysian Space Agency, in 2014, 2013, 2010, and 2009, and the Best Paper Presentation Award, in 2012, International Symposium on Antennas and Propagation (ISAP 2012) at Nagoya, Japan, and in 2015 in IconSpace, Malaysia. He was an Associate Editor of *IET Electronics Letter*. He also serves as the Guest Editor for *Sensors* Journal, and an Associate Editor for IEEE Access.

NORSUZLIN MOHD SAHAR was born in Melaka, Malaysia. She received the B.Eng. degree in communication engineering from International Islamic University Malaysia (IIUM), in 2006, the M.Eng. degree from Universiti Teknologi Malaysia (UTM), in 2010, and the Ph.D. degree for research in reconfigurable antenna using RF MEMs switches for RFID and GPS applications from Universiti Kebangsaan Malaysia (UKM), in 2016. She held the lecturing position at USCI University, Kuala Lumpur, and SEGi University, for more than ten years. She is currently a Senior Lecturer with the Space Science Centre (ANGKASA), Institute of Climate Change, UKM. Her research interests include the microwave device for wireless applications and systems particularly in broadband microstrip antennas and reconfigurable antennas.

KAMARULZAMAN MAT was born in Kedah, Malaysia. He received the B.Eng. degree from Universiti Kebangsaan Malaysia (UKM), in 1996, and the M.Sc. degree from Loughborough University, U.K. He is currently a Senior Lecturer with the Faculty of Engineering and Built Environment, Universiti Kebangsaan Malaysia. His research interests include active antenna, reflectarray antenna, and antenna design for medical applications.

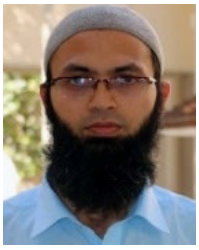

MUHAMMAD E. H. CHOWDHURY (Member, IEEE) received the B.Sc. and M.Sc. degrees (Hons.) from the Department of Electrical and Electronics Engineering, University of Dhaka, Bangladesh, and the Ph.D. degree from the University of Nottingham, U.K., in 2014. He worked as a Postdoctoral Research Fellow and a Hermes Fellow with the Sir Peter Mansfield Imaging Centre, University of Nottingham. He is currently working as a full-time Faculty with the Department of Electrical Engineering, Qatar University. Before joining Qatar University, he worked in several universities in Bangladesh. He has a patent and published around 60 peer-reviewed journal articles, conference papers, and two book chapters. He is also running several NPRP and UREP grants from QNRF and internal grants from Qatar University along with academic and government projects. He has been involved in EPSRC, ISIF, and EPSRC-ACC grants along with different national and international projects. He has worked as a consultant for the projects entitled, Driver Distraction Management Using Sensor Data Cloud (2013–2014, Information Society Innovation Fund (ISIF), Asia). His current research interests include biomedical instrumentation, signal processing, wearable sensors, medical image analysis, machine learning, embedded system design, and simultaneous EEG/fMRI. He is an Active Member of IEEE, British Radiology, Institute of Physics, ISMRM, and HBM. He received ISIF Asia Community Choice Award 2013 for a project entitled Design and Development of Precision Agriculture Information System for Bangladesh. He has recently won the COVID-19 dataset award for his contribution to fight against COVID-19. He is serving as an Associate Editor for IEEE Access and a Review Editor for Frontiers in *Neuroscience*.

HATEM RMILI (Senior Member, IEEE) received the B.S. degree in general physics from the Faculty of Science of Monastir, Tunisia, in 1995, the Diplôme d'études approfondies (DEA) Diploma degree in quantum mechanics from the Faculty of Science of Tunis, Tunisia, in 1999, and the Ph.D. degree in physics (electronics) from the University of Tunis, Tunisia, and the University of Bordeaux 1, France, in 2004. From December 2004 to March 2005, he was a Research Assistant with the PIOM Laboratory, University of Bordeaux 1. From March 2005 to March 2007, he was a Postdoctoral Fellow with the Rennes Institute of Electronics and Telecommunications, France. From March to September 2007, he was a Postdoctoral Fellow with the ESEO Engineering School, Angers, France. From September 2007 to August 2012, he was an Associate Professor with the Department of Electronics and Telecommunications, Mahdia Institute of Applied Science and Technology (ISSAT), Tunisia. He is currently a Full Professor with the Department of Electrical and Computer Engineering, Faculty of Engineering, King Abdulaziz University, Jeddah, Saudi Arabia. His research interests include applied electromagnetic applications involving antennas, metamaterials, and métasurfaces. The main targeted applications are reconfigurable antennas for multi-standard wireless communications systems, the security of chipless RFID systems with fractal tags, terahertz photoconductive antennas for infra-red energy harvesting, UWB nano rectennas for collection of solar energy, phase shifters for low-cost 5G communication systems, and microwave absorbing materials for stealth technologies.